Polymers **2013**, *5*, 1041-1055; doi:10.3390/polym5031041

OPEN ACCESS

polymers

ISSN 2073-4360

www.mdpi.com/journal/polymers

Article

DNA-Promoted Auto-Assembly of Gold Nanoparticles: Effect of the DNA Sequence on the Stability of the Assemblies

Matthieu Doyen, Kristin Bartik and Gilles Bruylants *

Engineering of Molecular NanoSystems, Ecole polytechnique de Bruxelles, CP 165/64, Université libre de Bruxelles, 50 av. F.D. Roosevelt, Brussels 1050, Belgium;
E-Mails: mdoyen@ulb.ac.be (M.D.); kbartik@ulb.ac.be (K.B.)

* Author to whom correspondence should be addressed; E-Mail: gbruylan@ulb.ac.be; Tel.: +32-2-6503586; Fax: +32-2-6503606.

Received: 26 June 2013; in revised form: 12 July 2013 / Accepted: 15 July 2013 / Published: 22 July 2013

Abstract: The use of deoxyribonucleic acid (DNA) oligonucleotides has proven to be a powerful and versatile strategy to assemble nanomaterials into two (2D) and three-dimensional (3D) superlattices. With the aim of contributing to the elucidation of the factors that affect the stability of this type of superlattices, the assembly of gold nanoparticles grafted with different DNA oligonucleotides was characterized by UV-Vis absorption spectroscopy as a function of temperature. After establishing an appropriate methodology the effect of (i) the length of the grafted oligonucleotides; (ii) the length of their complementary parts and also of (iii) the simultaneous grafting of different oligonucleotides was investigated. Our results indicate that the electrostatic repulsion between the particles and the cooperativity of the assembly process play crucial roles in the stability of the assemblies while the grafting density of the oligonucleotide strands seems to have little influence.

Keywords: gold nanoparticles; oligonucleotides; superlattices; thermal stability; UV-Vis absorption spectroscopy

1. Introduction

Many efforts have been devoted over recent years to the production of both two (2D) and three-dimensional (3D) superlattices of metallic, insulating or semiconducting nanoparticles [1–3]. These lattices can be considered as artificial crystals in which nanocrystals take the place of the atoms

in traditional crystals. This new class of materials is considered for a wide range of advanced applications, including information-storage, optoelectronics, catalysis and sensing [3–6]. By varying the nature, size or shape of the nanocrystals and their 2D or 3D organization, a vast diversity of materials with tunable properties can be envisaged. Furthermore, new collective electric, magnetic and optical properties can emerge from the ordered periodic arrangement which are dependent on the characteristics of the nanocrystals but also on the inter-particle distance and the nature of the functionalizing ligands [4,7]. It has for example been shown that the ordering of silver and gold nanoparticles into closely spaced 2D and 3D superlattices leads to the appearance of a strong and sharp collective plasmon resonance band [2,8–11].

Several strategies can be adopted to promote the formation of structured nanoparticle superlattices such as the anchoring of alkanethiols on gold nanoparticles [11,12]. In this case the non-directional London interactions between the alkanes will lead to the formation of the lattice. The use of deoxyribonucleic acid (DNA) oligonucleotides has proven to be a powerful and versatile strategy, developed since the mid-1990s [13,14], to assemble nanomaterials. This strategy takes advantage of the remarkable properties of these biomolecules, *i.e.*, the pairing selectivity and specificity of the DNA oligonucleotides, and the regular helical structure of double stranded DNA. This methodology represents a powerful tool for the engineering of superlattices, the particles providing the physical properties and the organic part controlling the auto-assembly process, as the assembly process can be precisely controlled and allows the assembly of different types of nanomaterials. Binary networks of particles varying in size [15] or nature [3,16,17] have for example been formed.

Essentially two groups, those of Chad Mirkin at the Northwestern University [13,15,16,18–29] and of Oleg Gang at the Brookhaven National Laboratory [17,30–35] have driven the research in the design of nanostructured materials using the programmable assembly properties of DNA. Most of the studies were undertaken with oligonucleotide functionalized gold nanoparticles (AuNP) with the aim to identify the parameters which control the type of structure obtained. The size of the AuNP, the oligonucleotide sequence and length as well as the surface density of oligonucleotides have been shown to play an important role [21,28,29,36]. The crystallization process has been shown to proceed via a 3-step mechanism: the nanoparticles are first randomly assembled into disordered aggregates which undergo a localized reorganization to form crystalline domains growing into well-ordered crystals [26].

It has been shown that the ionic strength of the solution, which is known to influence the stability of oligonucleotide duplexes, also influences the stability of the AuNP-DNA aggregates [29]. However, a clear understanding of the effect of the grafting of oligonucleotides on AuNP on the stability of the structures that they form requires further investigation. Very few studies have been devoted to the characterization of the stability of the assemblies at the molecular level, *i.e.*, by comparison with the pairing stability of the equivalent free (non-grafted) oligonucleotides. The work reported here was undertaken with AuNP directly functionalized with oligonucleotides presenting complementary parts (see Figure 1) without using linkers (a oligonucleotide sequence which has two parts, each one complementary to the sequence grafted on a AuNP). The linker strategy is used in most of the studies devoted to superlattices formation; however, it introduces additional parameters (linker concentration, nucleotidic sequence of the linker, *etc.*) which further complicates the comparison of the stability of the assemblies with that of the free oligonucleotides. We report here on the effect of different experimental parameters and of different characteristics of the grafted nucleotide sequences on the stability of assemblies.

Figure 1. Schematic representation of the assembly of two sets of nanoparticles functionalized with oligonucleotides with complementary segments.

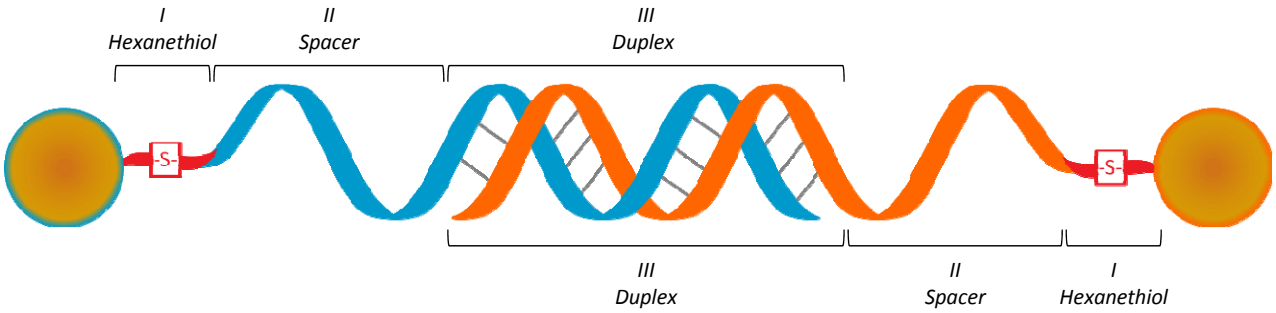

2. Experimental Section

2.1. Synthesis of AuNP

Gold nanoparticle synthesis was based on an optimized Turkevich method [37,38]. All solutions were prepared with HPLC grade water (Sigma Aldrich, St. Louis, MO, USA). Glassware was soaked prior to use in aqua regia (25% HNO_3, 75% HCl) and thoroughly rinsed with milli-Q water. 1 mL of trisodium citrate solution ($Na_3C_6H_5O_7$, Alfa Aesar, Karlsruhe, Germany) was injected into 50 mL of boiling aqueous tetrachloroauric solution ($KAuCl_4$, Sigma Aldrich, St. Louis, MO, USA), both adjusted at pH = 7. Concentrations were chosen so as to achieve a final concentration of 0.3 mM in $AuCl_4^-$ with a citrate to gold ratio of 5. AuNP were analyzed by transmission electron microscope (TEM), Philips CM20-UltraTWIN equipped with a lanthanum hexaboride (LaB_6) crystal at 200 kV accelerating voltage, and a mean size of 15 nm was determined.

2.2. Functionalization of AuNP

Gold nanoparticles were functionalized with oligonucleotides using procedures described in the literature [22]. The thiol-modified (hexanethiol modification) oligonucleotides (Integrated DNA Technologies, Leuven, Belgium) were mixed with 0.1 M dithiothreitol (DTT, Sigma Aldrich, St. Louis, MO, USA) in a phosphate buffer solution (PB, pH 8.0) to cleave the disulfide bond. After 1 h, the oligonucleotides were purified using a desalting PD-10 column (Sephadex G-25 medium, GE Healthcare, Diegem, Belgium) and directly added to the solution of AuNP (approximately 4 nmol of oligonucleotides per mL). The solution was mixed at room temperature for 20 min before stepwise addition of a NaCl solution to obtain a final salt concentration of 1 M (0.05 M, 0.1 M and every 0.1 M increment to 1 M). Between two additions the solution was sonicated during 10 s and left under agitation for 20 min at room temperature. Once the final salt concentration was reached, the solution was left under agitation overnight at room temperature. In order to remove the excess of oligonucleotides the AuNP solution was centrifuged, the supernatant was removed and the AuNP-DNA were redispersed in water. This was done five times. After the final round, AuNP-DNA were redispersed in the desired buffer (typically 10 mM phosphate, pH 7.4, 500 mM NaCl). Different sets of AuNP-DNA were prepared with the oligonucleotides presented in Table 1. Each oligonucleotide was composed of (see Figure 1): (i) a thiol anchoring moiety; (ii) a spacer and (iii) the segment which is involved in the formation of the duplex when two sets of complementary functionalized AuNP-DNA are mixed. In has

been shown in the case of mixtures, that the surface density of an oligonucleotide is proportional to its mole fraction in solution [22].

Table 1. Acronym and sequence of the oligonucleotides used to functionalize the gold nanoparticles (AuNP).

Acronym	Sequence
$DNAA_{11}$	thiolC6-5′-CGCACACACGC-3′
$DNAT_{11}$	thiolC6-5′-GCGTGTGTGCG-3′
$T10\text{-}DNAA_{11}$	thiolC6-5′-TTTTTTTTTTCGCACACACGC-3′
$A10\text{-}DNAA_{11}$	thiolC6-5′-AAAAAAAAAACGCACACACGC-3′
$T10\text{-}DNAT_{11}$	thiolC6-5′-TTTTTTTTTTGCGTGTGTGCG-3′
$A10\text{-}DNAT_{11}$	thiolC6-5′-AAAAAAAAAAGCGTGTGTGCG-3′
$T10\text{-}DNAA_5$	thiolC6-5′-TTTTTTTTTTCGCAC-3′
$T10\text{-}DNAT_5$	thiolC6-5′-TTTTTTTTTTGCGTG-3′

2.3. Assembly of AuNP-DNA

Solutions of AuNP-DNA functionalized with oligonucleotides showing complementary segments dispersed in the desired buffer were mixed. Concentrations of AuNP-DNA were determined using an extinction coefficient of 3×10^9 M^{-1} cm^{-1} for AuNP of 15 nm at the maximum absorption of their surface plasmon resonance band (518 nm). Volumes were chosen so as to have equal concentrations in both types of AuNP-DNA. UV-Vis spectra were recorded between 200 and 800 nm at a 240 nm/min scan rate or followed at 260 nm in function of temperature, with a heating or cooling rate of 0.1, 0.5 or 1 °C/min, on a Lambda-35 Perkin-Elmer spectrophotometer equipped with a PTP-1 temperature controller.

3. Results and Discussion

The AuNP were synthesized, as described above, and characterized by UV-Vis absorption spectroscopy and TEM. They display a SPR band maximum at 518 nm consistent with the mean size of 15 nm measured by TEM [39]. The AuNP were functionalized with different oligonucleotides according to procedures described in the literature [22] which leads to an 8 nm hypsochrome shift of the SPR band. These functionalized AuNP could be precipitated and easily redispersed without any change of their absorption spectrum, which is not the case when citrate is used as protecting agent. The oligonucleotide sequences chosen were all based on an 11-mer that has previously been characterized both from a structural and a thermodynamic points of view [40,41]. The 11-mer is known to form a B-DNA turn and its melting temperature, T_m, temperature at which half of the strands are in a single strand state, has been determined for a large range of duplex and salt concentrations.

AuNP functionalized with complementary oligonucleotides were mixed in equal quantities and the stability of the different assemblies was monitored by UV-Vis absorption spectroscopy as a function of temperature. Figure 2 presents the evolution of the absorption at 260 nm for a solution obtained by mixing AuNP functionalized with the $DNA\text{-}A_{11}$ and $DNA\text{-}T_{11}$ sequences (see Table 1). Several consecutive temperature cycles give totally superimposable results showing the total reversibility of the process. Sharp transitions in absorbance are observed for all the systems studied, both upon heating

and cooling which is not the case for AuNP-DNA which have not been paired with their complementary particles. This clearly shows that the transition is a signature of the association of the nanoparticles. The change in absorption is not due to the change in the absorbance of the oligonucleotides with temperature as their contribution to the total absorption is negligible. Indeed, on the basis of data reported in the literature, the numbers of strands on the nanoparticles can be estimated to be between 340 and 580 [12,14] and taking into account the molar extinction coefficients of AuNP at 260 nm (of the order of 10^9 M^{-1} cm^{-1}) and of oligonucleotides (of the order of 10^5 M^{-1} cm^{-1} [41]), the fraction of the absorption due to oligonucleotides is less than 2% of the total absorption at this wavelength.

Figure 2. Absorbance at 260 nm as a function of temperature of a solution of AuNP-DNAA_{11} mixed with AuNP-DNAT_{11}. Three assembly/disassembly cycles are displayed.

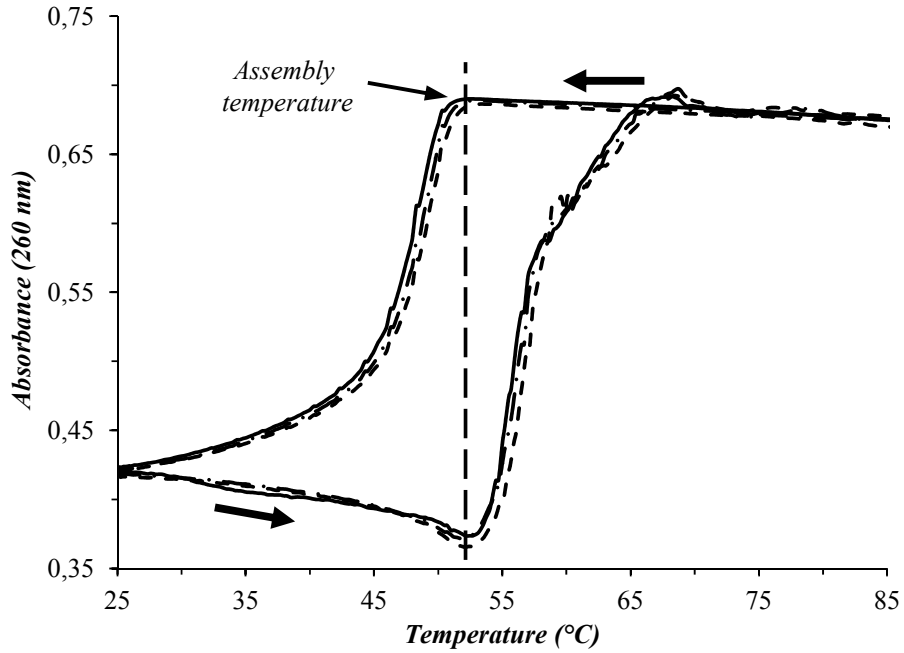

The cycle observed in Figure 2 can be explained as follows: starting from high temperatures, at which the AuNP-DNA are dispersed, a sharp decrease in absorbance is observed upon cooling when the oligonucleotides start pairing and the assemblies form. When AuNP-DNA associate an hypsochrome shift of the maximum of the Surface Plasmon Resonance (SPR) band is observed, which leads to a decrease in absorbance at 260 nm (and an increase at wavelengths above 526 nm; see Appendix, Figure A1). As the assemblies become larger, they start to precipitate, which leads to a further decrease in absorbance, in this case at all wavelengths. Should the system be left at room temperature at the end of the cooling ramp, the absorbance will drop to zero when all the assemblies have precipitated. If the temperature ramp is inverted immediately, which is the case for the data reported in Figure 2, the absorbance first decreases slightly due to some additional precipitation but when the oligonucleotides start to unpair, the particles dissociate and are redispersed which leads to a sharp increase of the absorbance to its initial value. The sharpness of this transition clearly indicates that the dissociation process of the AuNP-DNA is a cooperative process. Circular Dichroïsm (CD) and fluorescence measurements reported in the literature highlight that the DNA duplexes formed between oligonucleotides grafted on AuNP melt in a highly cooperative manner and that the melting transitions

observed is the signature of the entire melting process [21]. The hysteresis observed can be explained by the fact that the system is not at thermodynamic equilibrium during the cooling and heating process. In order to be able to compare the stability of different systems; it is important to decide which characteristic point in the cycle can be compared.

The dissociation/association process of AuNP-DNA functionalised with the complementary T_{10}-$DNAA_{11}$ and T_{10}-$DNAT_{11}$ strands was studied at different heating/cooling rates (1 °C/min, 0.5 °C/min and 0.1 °C/min) and the results are displayed in Figure 3. The hysteresis is more pronounced when the temperature ramp is faster with the process monitored upon cooling the most affected. This is due to the fact that, as known for free oligonucleotides (*i.e.*, oligonucleotides not anchored on AuNP), the paring rate is slow and, upon fast cooling, the system is far from thermodynamic equilibrium [42,43] but is also due to the fact that precipitation is kinetically controlled. This latter effect explains why the absorbance at 25 °C is different for the different temperature ramps. For all the reasons mentioned above, the quantitative analysis of the heating/cooling curves using the classical thermodynamic model for the denaturation of free duplexes is not suited for the analysis of the dissociation/association of AuNP-DNA assemblies and should not be used to characterize these systems. The temperature at which the absorbance starts to decrease is the same for all temperature ramps and is furthermore very close to the temperature at which the absorbance starts to increase upon heating.

Figure 3. Absorbance at 260 nm as a function of temperature during assembly and disassembly cycle of complementary AuNP-DNA (AuNP-T10-$DNAA_{11}$ mixed with AuNP-T10-$DNAT_{11}$) recorded using three different heating/cooling rates: 1 °C/min (dashed line); 0.5 °C/min (solid line); 0.1 °C/min (bold line).

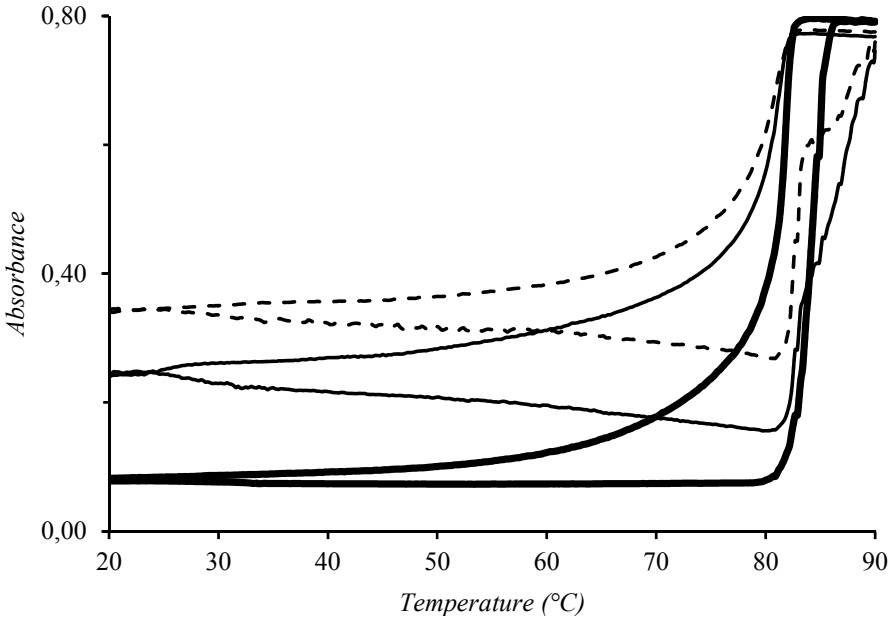

It was decided to characterize the stability of the assemblies by the temperature at which the absorbance starts to decrease upon cooling. This temperature, characteristic of the assembly process, is given in Table 2 for all the systems that were studied. The assumption can be made that systems with a higher assembly temperature can be considered as more stable at room temperature, assumption which is also made in the case of free oligonucleotides where a higher melting temperature (T_m) is considered

to be the signature of a thermodynamically more stable duplex [40,42]. The assembly temperature however cannot be directly compared to the T_m of the free oligonucleotides as it is not the same process which is being monitored. As already mentioned, the change in absorption upon heating/cooling is not due to the pairing/dissociation of the oligonucleotides but to the shift of the SPR band of the nanoparticles and to their dispersion/precipitation.

Table 2. Characteristic assembly temperature (±1 °C) of the different systems obtained by mixing AuNP with complementary oligonucleotide strands.

System No.	AuNP-DNA-1	AuNP-DNA-2	$T_{Assembly}$ (°C)
1	$DNAA_{11}$	$DNAT_{11}$	52
2	$DNAA_{11}$	T10-$DNAT_{11}$	72
3	T10-$DNAA_{11}$	T10-$DNAT_{11}$	82
4	T10-$DNAA_{11}$	T10-$DNAT_5$	64
5	T10-$DNAA_5$	T10-$DNAT_{11}$	61
6	T10-$DNAA_{11}$/T10-$DNAA_5$ (25/75)	T10-$DNAT_{11}$	85
7	T10-$DNAA_{11}$/T10-$DNAA_5$ (50/50)	T10-$DNAT_{11}$	84
8	T10-$DNAA_{11}$/T10-$DNAA_5$ (75/25)	T10-$DNAT_{11}$	85

The assembly temperature of AuNP functionalized with the same complementary 11-mer strands but anchored on the nanoparticles via spacers of different lengths (systems 1, 2 and 3) highlights that the distance between the metallic cores affects the stability of the assembly (see also Appendix, Figure A2). Assuming the formation of B-DNA strands, the distance can roughly be estimate to range from 5 to 12 nm going from system 1 to 3. Identical results were obtained when the spacers were composed of adenines indicating that the nature of the spacer does not influence the stability of the assemblies (see Appendix, Table A1). With the shortest spacers (system 1), the assembly temperature is lower than the melting temperature determined for the free duplex. The T_m of the 11-mer in a 500 mM NaCl solution ranges between 60 and 70 °C depending on oligonucleotide concentration (see Appendix, Figures A3 and A4). For the longest spacers (system 3) the temperature is far above the T_m which indicates that, even if the two temperatures cannot be directly compared as they do not characterize exactly the same processes, the AuNP can assemble at temperatures at which the free duplex is totally unpaired. The increase in stability with distance could be due to a larger number of duplexes formed between two AuNP, thanks to the higher flexibility of the strands. Electrostatic repulsion between particles is certainly also an important factor as evidenced by the fact that a high salt concentration (500 mM), which screens electrostatic interactions, is required to observe the formation of the assemblies. Mirkin *et al*. have reported that particle-particle repulsion, which is sensitive to the interparticle distance, is a dominant factor which affects the stability of AuNP-DNA assemblies [21]. It has also been reported in the literature that a higher stability of the assemblies could be the result of an increase in the stability of the oligonucleotide duplexes due to higher local ionic strengths [21]. However, ITC results highlight that the anchoring of one of the strands on AuNP does not influence the thermodynamics of duplex formation with its complementary strand (same $\Delta H°$ and $\Delta G°$ as for free oligonucleotides) [44] suggesting that this is maybe not the dominant factor. The smaller loss of entropy (translational and rotational degrees of freedom) upon simultaneous pairing of multiple strands anchored on the AuNP, compared to the situation where all the strands are free in

solution, will certainly have a positive effect on the stability of the ensemble, as already shown in numerical studies reported in the literature [45].

The stability of two systems with shorter complementary strands (5-mers) was also investigated (systems 4 and 5, see Appendix, Figure A5) and their assembly temperatures were found to be essentially the same and approximately 20 °C lower than that of the assembly formed with the 11-mer for a same interparticle distance (system 3). The stability of the equivalent free 5-mer is predicted to be around 34 °C under similar experimental conditions [46]. With the 5-mers the assemblies also form at temperatures well above the T_m. This confirms that the cooperative pairing of the anchored nucleotides plays a major role on the stability of the assemblies.

The stability of systems for which one set of AuNP is functionalized with mixtures of T10-DNAA$_{11}$ and T10-DNAA$_5$ oligonucleotides in respective ratios of 100/0, 75/25, 50/50, 25/75 and 0/100 and paired with AuNP functionalized with the T10-DNAT$_{11}$ oligonucleotide was also investigated (see Figure 4). The simultaneous pairing of T10-DNAA$_{11}$ and T10-DNAA$_5$ anchored on the same NP is possible as both should lead to the same distance between the Au cores when paired with the T10-DNAT$_{11}$ strand. Surprisingly, all the systems which contain a certain proportion of the T10-DNAA$_{11}$ strands display the same transition temperature which is well above the stability of the system containing only the T10-DNAA$_5$ strand. This clearly highlights the pairing process is controlled by the strands that display the higher stability, *i.e.*, those who have the longest complementary parts, whatever their surface density. It is interesting to make the link here with the results mentioned above concerning the use of poly-A instead of poly-T to anchor the oligonucleotides onto the AuNP, which show that the systems have the same assembly temperature (see Appendix, Table A1) even if, as reported in the literature, poly-A leads to lower grafting densities [12,14].

Figure 4. Normalized absorbance at 260 nm during assembly of AuNP functionalized with T10-DNAT$_{11}$ and mixed AuNP functionalized with (i) T10-DNAA$_{11}$ (plain); (ii) T10-DNAA$_{11}$/T10-DNAA$_5$ (25/75) (dotted); (iii) T10-DNAA$_{11}$/T10-DNAA$_5$ (50/50) (dotted-point); (iv) T10-DNAA$_{11}$/T10-DNAA$_5$ (75/25) (dotted-double point) and (v) T10-DNAA$_5$ (bold) in function of temperature.

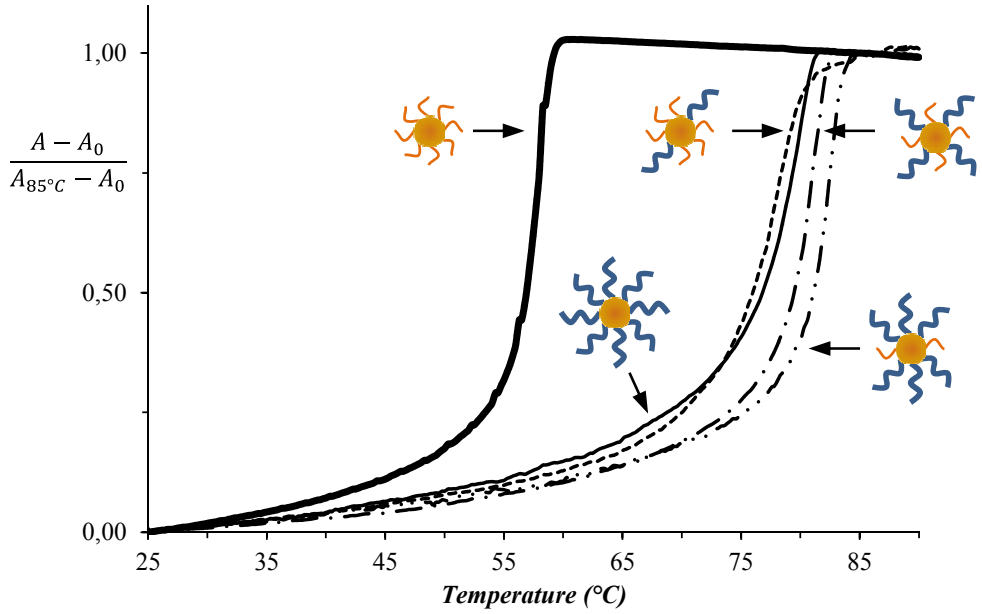

4. Conclusions

With the aim of contributing to the elucidation of the factors that affect the stability of AuNP-DNA superlattices, the assembly of AuNP grafted with different DNA oligonucleotides was characterized by UV-Vis absorption spectroscopy as a function of temperature. The temperature at which the assemblies start to form upon cooling was used to compare the different systems. This temperature was observed to be independent of the heating and cooling rates. The effect of the length of the grafted oligonucleotides and of the length of their complementary parts on the stability of the assemblies was investigated. The stability of systems where oligonucleotides with complementary strands of different lengths were grafted on the same AuNP was also investigated.

Our results indicate that the distance between the particles has a marked effect on the stability of the assembly. For the system leading to the smallest interparticle distance (around 5 nm), no assemblies are formed in a 100 mM NaCl phosphate buffer, conditions in which the free duplexes are perfectly stable, and at high ionic strength (500 mM NaCl) the lattices are less stable than the duplexes formed by the free equivalent oligonucleotide strands. All this shows that the electrostatic repulsion between the particles has a destabilizing effect on the assembly process. At equal interparticle distance the assemblies are more stable when the AuNP are linked by longer complementary strands, highlighting the effect of the intrinsic stability of the duplex. The fact that the assembly temperatures of these systems are considerably higher than the T_m of the corresponding free duplexes, is a clear indication that the assembly process is highly cooperative. Experiments undertaken with AuNP grafted with oligonucleotides of different lengths indicate that the grafting density of the oligonucleotide strands seems to have little effect on the stability of the assemblies.

In conclusion, our study shows that, if the intrinsic stability of the oligonucleotide duplex used to pair the AuNP affects the stability of the assemblies, the electrostatic repulsion between the nanoparticles and the cooperativity of the assembly process are the key factors that need to be considered when programming the auto-assembly of nanoparticles superlattices using DNA oligonucleotides.

Acknowledgments

M.D. thanks the FRIA for a doctoral fellowship. G.B. and K.B. thank the Belgian FRS-FNRS for funding (FRFC 2.4592.10; CDR 14505386).

Conflict of Interest

The authors declare no conflict of interest.

Appendix

Figure A1. Absorption spectra during the cooling ramp of the assembly AuNPs-$DNAA_{11}$ mixed with AuNPs-$DNAT_{11}$.

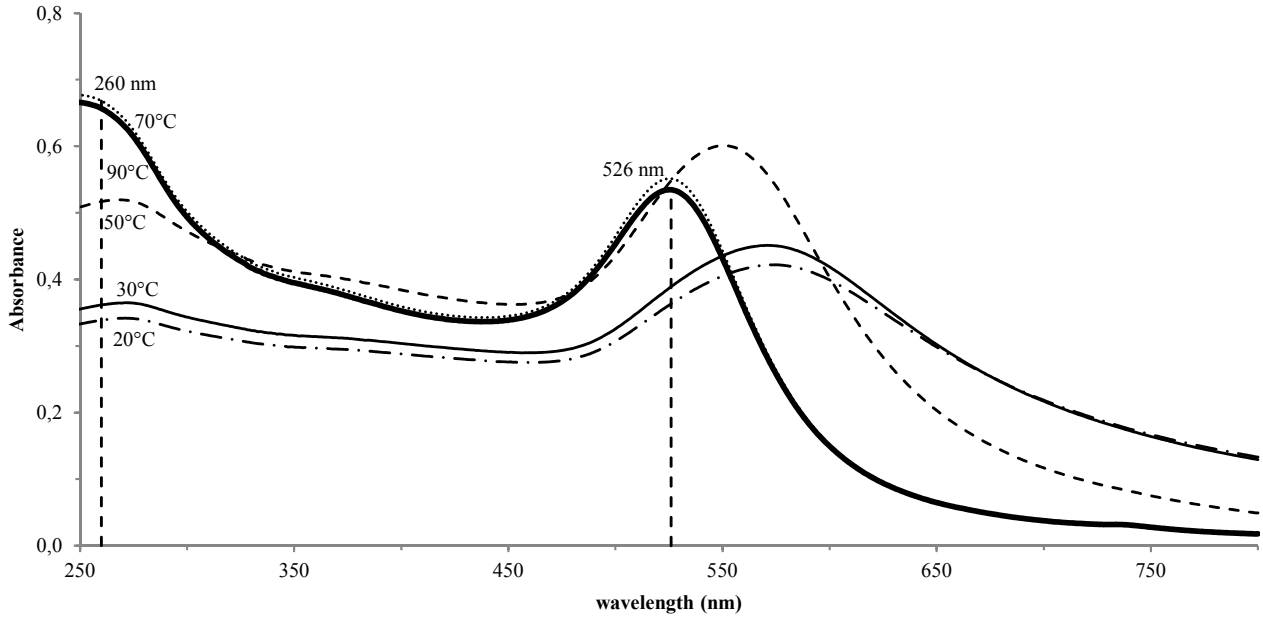

Figure A2. Normalized absorbance at 260 nm during assembly of DNA-AuNPs functionalized with the complementary oligonucleotides $DNAA_{11}$ & $DNAT_{11}$ (plain), $DNAA_{11}$ & T10-$DNAT_{11}$ (dotted) and T10- $DNAA_{11}$ & T10- $DNAT_{11}$ (bold) as a function of temperature.

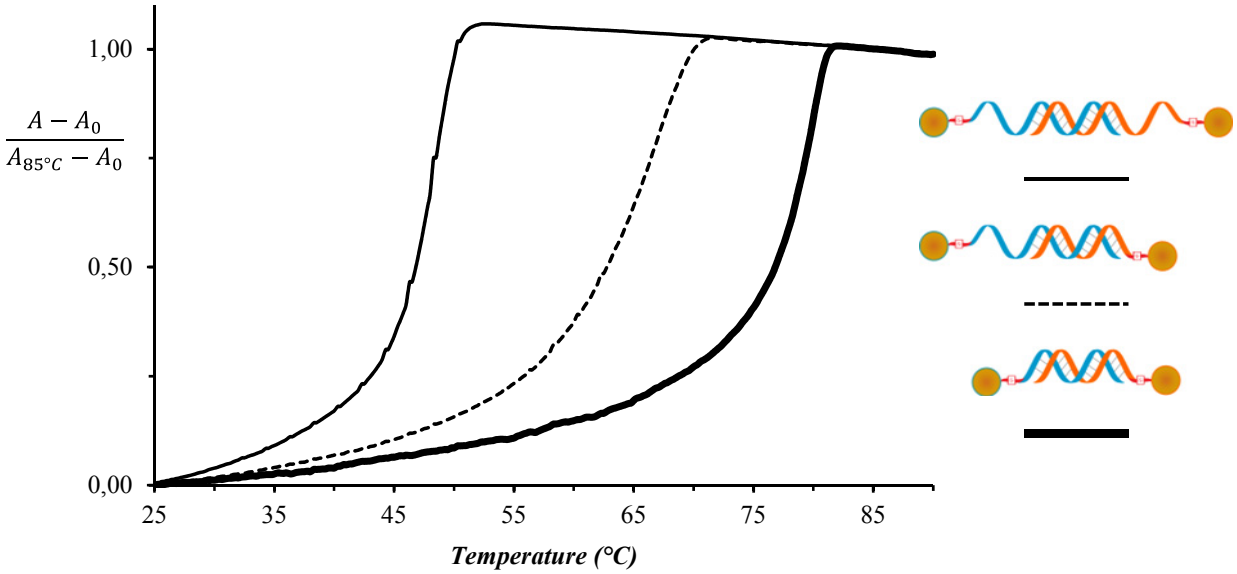

Table A1. Characteristic assembly temperature (±1 °C) of the different systems obtained by mixing AuNPs with complementary oligonucleotide strands.

System No.	DNA-AuNP-1	DNA-AuNP-2	$T_{Assembly}$ (°C)
1	$DNAA_{11}$	$DNAT_{11}$	52
2	$DNAA_{11}$	T10-$DNAT_{11}$	72
3	T10-$DNAA_{11}$	T10-$DNAT_{11}$	82
	A10-$DNAA_{11}$	A10-$DNAT_{11}$	82
	T10-$DNAA_{11}$	A10-$DNAT_{11}$	82
	A10-$DNAA_{11}$	T10-$DNAT_{11}$	82
4	T10-$DNAA_{11}$	T10-$DNAT_5$	64
5	T10-$DNAA_5$	T10-$DNAT_{11}$	61
6	T10-$DNAA_{11}$/T10-$DNAA_5$ (25/75)	T10-$DNAT_{11}$	85
7	T10-$DNAA_{11}$/T10-$DNAA_5$ (50/50)	T10-$DNAT_{11}$	84
8	T10-$DNAA_{11}$/T10-$DNAA_5$ (75/25)	T10-$DNAT_{11}$	85

Figure A3. Thermal denaturation curve of the DNAA11-DNAT11 duplex (5 µM) followed by UV-Vis absorption spectroscopy at 260 nm in a 10 mM phosphate buffer containing 500 mM NaCl at pH = 7.4.

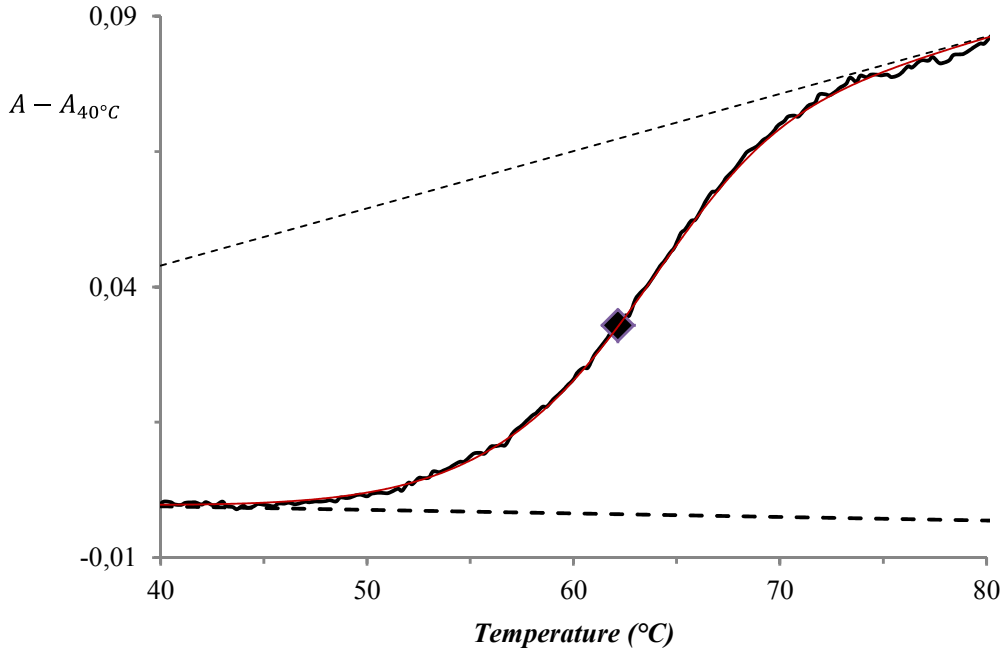

Figure A4. Mean value of melting temperature and a confidence interval of 95% in a 100 mM NaCl(diamond), melting temperature in a 500 mM NaCl (square), predicted melting temperature in a 100 mM NaCl (plain) and predicted melting temperature in a 500 mM (bold) of the pairing between strands A_{11} & T_{11} in function of duplex concentration. Prediction were made with *OligoCalc* [46].

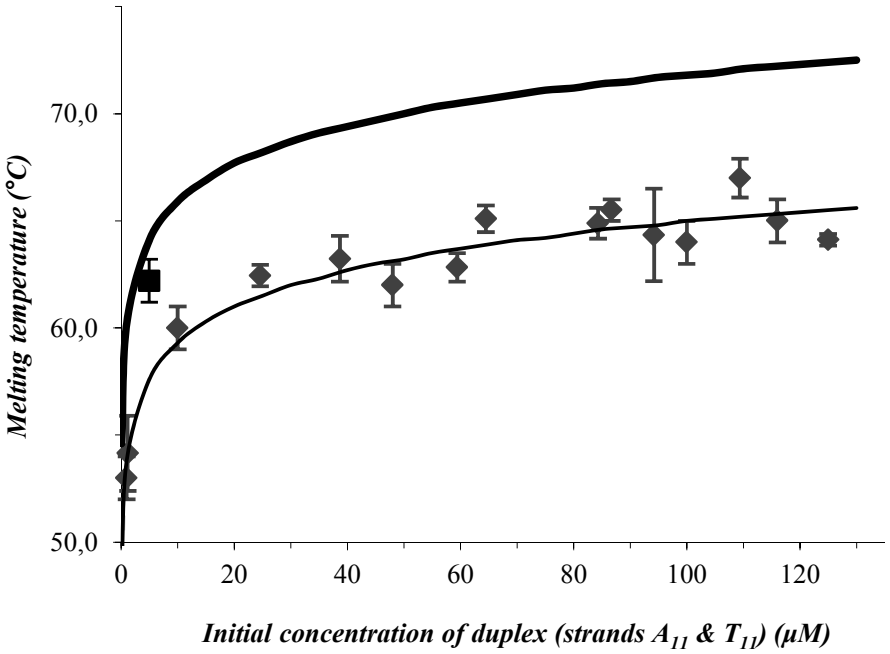

Figure A5. Normalized absorbance at 260 nm during the assembly of DNA-AuNPs functionalized with the complementary strands T10-DNAA_{11} & T10-DNAT_{11} (plain), T10 DNAA_{11} & T10-DNAT_5 (dotted), and T10 DNAA_5 & T10-DNAT_{11} (bold) as a function of temperature.

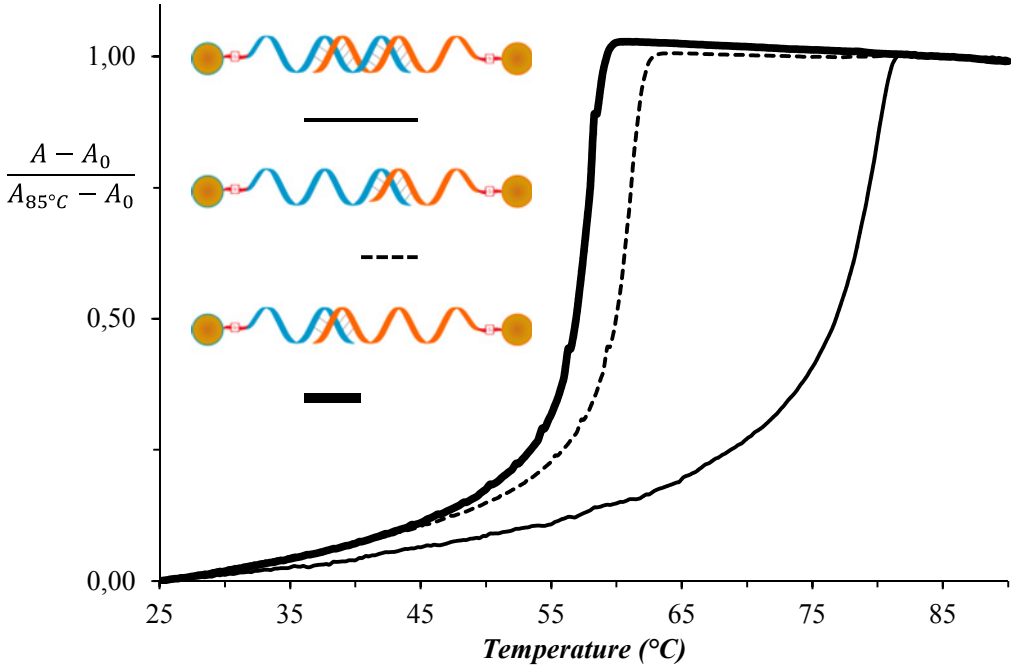

References

1. Talapin, D.V. LEGO Materials. *ACS Nano* **2008**, *2*, 1097–1100.
2. Pileni, M.P. Supracrystals of inorganic nanocrystals: An open challenge for new physical properties. *Acc. Chem. Res.* **2008**, *41*, 1799–1809.
3. Shevchenko, E.V.; Talapin, D.V.; Kotov, N.A.; O'Brien, S.; Murray, C.B. Structural diversity in binary nanoparticle superlattices. *Nature* **2006**, *439*, 55–59.
4. Urban, J.J.; Talapin, D.V.; Shevchenko, E.V.; Kagan, C.R.; Murray, C.B. Synergism in binary nanocrystal superlattices leads to enhanced p-type conductivity in self-assembled PbTe/Ag_2Te thin films. *Nat. Mater.* **2007**, *6*, 115–121.
5. Bruylants, G.; Bartik, K.; Delplancke-Ogletree, M.-P. Growth Kinetics and Controlled Auto-Assembly of Gold Nanoparticles. In Proceedings of the European Conference on Nano-Films, Liège, Belgium, 24 March 2010; p. 5.
6. Hutter, E.; Fendler, J.H. Exploitation of localized surface plasmon resonance. *Adv. Mater.* **2004**, *16*, 1685–1706.
7. Kalsin, A.M.; Fialkowski, M.; Paszewski, M.; Smoukov, S.K.; Bishop, K.J.M.; Grzybowski, B.A. Electrostatic self-assembly of binary nanoparticle crystals with a diamond-like lattice. *Science* **2006**, *312*, 420–424.
8. Taleb, A.; Russier, V.; Courty, A.; Pileni, M. Collective optical properties of silver nanoparticles organized in two-dimensional superlattices. *Phys. Rev. B* **1999**, *59*, 13350–13358.
9. Pinna, N.; Maillard, M.; Courty, A.; Russier, V.; Pileni, M. Optical properties of silver nanocrystals self-organized in a two-dimensional superlattice: Substrate effect. *Phys. Rev. B* **2002**, *66*, 045415:1–045415:6.
10. Pileni, M.P.; Lalatonne, Y.; Ingert, D.; Lisiecki, I.; Courty, A. Self assemblies of nanocrystals: Preparation, collective properties and uses. *Faraday Discuss.* **2004**, *125*, 251–264.
11. Chen, C.-F.; Tzeng, S.-D.; Chen, H.-Y.; Lin, K.-J.; Gwo, S. Tunable plasmonic response from alkanethiolate-stabilized gold nanoparticle superlattices: Evidence of near-field coupling. *J. Am. Chem. Soc.* **2008**, *130*, 824–826.
12. Sidhaye, D.S.; Prasad, B.L.V. Melting Characteristics of superlattices of alkanethiol-capped gold nanoparticles: The "excluded" story of excess thiol. *Chem. Mater.* **2010**, *22*, 1680–1685.
13. Mirkin, C.A.; Letsinger, R.L.; Mucic, R.C.; Storhoff, J.J. A DNA-based method for rationally assembling nanoparticles into macroscopic materials. *Nature* **1996**, *382*, 607–609.
14. Alivisatos, A.P.; Johnsson, K.P.; Peng, X.; Wilson, T.E.; Loweth, C.J.; Bruchez, M.P.; Schultz, P.G. Organization of 'nanocrystal molecules' using DNA. *Nat. Lett.* **1996**, *382*, 609–611.
15. Mucic, R.C.; Storhoff, J.J.; Mirkin, C.A.; Letsinger, R.L. DNA-directed synthesis of binary nanoparticle network materials. *J. Am. Chem. Soc.* **1998**, *120*, 12674–12675.
16. Mitchell, G.P.; Mirkin, C.A.; Letsinger, R.L. Programmed assembly of DNA functionalized quantum dots. *J. Am. Chem. Soc.* **1999**, *121*, 8122–8123.
17. Sun, D.; Gang, O. Binary heterogeneous superlattices assembled from quantum dots and gold nanoparticles with DNA. *J. Am. Chem. Soc.* **2011**, *133*, 5252–5254.
18. Storhoff, J.J.; Mirkin, C.A. Programmed materials synthesis with DNA. *Chem. Rev.* **1999**, *99*, 1849–1862.

19. Mirkin, C.A. Programming the assembly of two- and three-dimensional architectures with DNA and nanoscale inorganic building blocks. *Inorg. Chem.* **2000**, *39*, 2258–2272.
20. Demers, L.M.; Mirkin, C.A.; Mucic, R.C.; Reynolds, R.A.; Letsinger, R.L.; Elghanian, R.; Viswanadham, G. A fluorescence-based method for determining the surface coverage and hybridization efficiency of thiol-capped oligonucleotides bound to gold thin films and nanoparticles. *Anal. Chem.* **2000**, *72*, 5535–5541.
21. Jin, R.; Wu, G.; Li, Z.; Mirkin, C. What controls the melting properties of DNA-linked gold nanoparticle assemblies? *J. Am. Chem. Soc.* **2003**, *125*, 1643–1654.
22. Hurst, S.J.; Lytton-Jean, A.K.R.; Mirkin, C.A. Maximizing DNA loading on a range of gold nanoparticle sizes. *Anal. Chem.* **2006**, *78*, 8313–8318.
23. Park, S.Y.; Lytton-Jean, A.K.R.; Lee, B.; Weigand, S.; Schatz, G.C.; Mirkin, C.A. DNA-programmable nanoparticle crystallization. *Nature* **2008**, *451*, 553–556.
24. Hurst, S.J.; Hill, H.D.; Mirkin, C.A. "Three-dimensional hybridization" with polyvalent DNA-gold nanoparticle conjugates. *J. Am. Chem. Soc.* **2008**, *130*, 12192–12200.
25. Hill, H.D.; Macfarlane, R.J.; Senesi, A.J.; Lee, B.; Park, S.Y.; Mirkin, C.A. Controlling the lattice parameters of gold nanoparticle FCC crystals with duplex DNA linkers. *Nano Lett.* **2008**, *8*, 2341–2344.
26. Macfarlane, R.J.; Lee, B.; Hill, H.D.; Senesi, A.J.; Seifert, S.; Mirkin, C.A. Assembly and organization processes in DNA-directed colloidal crystallization. *PNAS* **2009**, *106*, 10493–10498.
27. Jones, M.R.; Macfarlane, R.J.; Lee, B.; Zhang, J.; Young, K.L.; Senesi, A.J.; Mirkin, C.A. DNA-nanoparticle superlattices formed from anisotropic building blocks. *Nat. Mater.* **2010**, *9*, 913–917.
28. Macfarlane, R.J.; Jones, M.R.; Senesi, A.J.; Young, K.L.; Lee, B.; Wu, J.; Mirkin, C.A. Establishing the design rules for DNA-mediated programmable colloidal crystallization. *Angew. Chem. Int. Ed. Engl.* **2010**, *122*, 4589–4592.
29. Macfarlane, R.J.; Lee, B.; Jones, M.R.; Harris, N.; Schatz, G.C.; Mirkin, C.A. Nanoparticle superlattice engineering with DNA. *Science* **2011**, *334*, 204–208.
30. Maye, M.M.; Nykypanchuk, D.; van der Lelie, D.; Gang, O. A simple method for kinetic control of DNA-induced nanoparticle assembly. *J. Am. Chem. Soc.* **2006**, *128*, 14020–14021.
31. Maye, M.M.; Nykypanchuk, D.; van der Lelie, D.; Gang, O. DNA-regulated micro- and nanoparticle assembly. *Small* **2007**, *3*, 1678–1682.
32. Nykypanchuk, D.; Maye, M.M.; van der Lelie, D.; Gang, O. DNA-based approach for interparticle interaction control. *Langmuir* **2007**, *23*, 6305–6314.
33. Xiong, H.; van der Lelie, D.; Gang, O. DNA linker-mediated crystallization of nanocolloids. *J. Am. Chem. Soc.* **2008**, *130*, 2442–2443.
34. Maye, M.M.; Kumara, M.T.; Nykypanchuk, D.; Sherman, W.B.; Gang, O. Switching binary states of nanoparticle superlattices and dimer clusters by DNA strands. *Nat. Nanotechnol.* **2010**, *5*, 116–120.
35. Xiong, H.; Sfeir, M.Y.; Gang, O. Assembly, structure and optical response of three-dimensional dynamically tunable multicomponent superlattices. *Nano Lett.* **2010**, *10*, 4456–4462.
36. Nykypanchuk, D.; Maye, M.M.; van der Lelie, D.; Gang, O. DNA-guided crystallization of colloidal nanoparticles. *Nat. Lett.* **2008**, *451*, 549–552.

37. Turkevich, J.; Stevenson, P.C.; Hillier, J. A study of the nucleation and growth processes in the synthesis of colloidal gold. *Discuss. Faraday Soc.* **1951**, *11*, 55–75.
38. Doyen, M.; Bartik, K.; Bruylants, G. UV-Vis and NMR study of the formation of gold nanoparticles by citrate reduction: Observation of gold-citrate aggregates. *J. Colloid Interface Sci.* **2013**, *399*, 1–5.
39. He, Y.Q.; Liu, S.P.; Kong, L.; Liu, Z.F. A study on the sizes and concentrations of gold nanoparticles by spectra of absorption, resonance Rayleigh scattering and resonance non-linear scattering. *Spectrochim. Acta A Mol. Biomol. Spectrosc.* **2005**, *61*, 2861–2866.
40. Bruylants, G.; Boccongelli, M.; Snoussi, K.; Bartik, K. Comparison of the thermodynamics and base-pair dynamics of a full LNA:DNA duplex and of the isosequential DNA:DNA duplex. *Biochemistry* **2009**, *48*, 8473–8482.
41. Cahen, P.; Luhmer, M.; Fontaine, C.; Morat, C.; Reisse, J.; Bartik, K. Study by ^{23}Na-NMR, ^{1}H-NMR, and ultraviolet spectroscopy of the thermal stability of an 11-basepair oligonucleotide. *Biophys. J.* **2000**, *78*, 1059–1069.
42. Cahen, P. Etude de l'atmosphère ionique et de la stabilité de la structure double brin d'oligonucléotides par RMN du ^{23}Na [in French]. Ph.D. Thesis, Université Libre de Bruxelles, Bruxelles, Belgium, 28 January 2000.
43. Braulin, W.H.; Bloomfield, V.A. 1H NMR study of the base-pairing reactions of d(GGAATTCC): Salt effects on the equilibria and kinetics of strand association. *Biochemistry* **1991**, *30*, 754–758.
44. Lang, B. Hybridization thermodynamics of DNA bound to gold nanoparticles. *J. Chem. Thermodyn.* **2010**, *42*, 1435–1440.
45. Largo, J.; Starr, F.W.; Sciortino, F. Self-assembling DNA dendrimers: A numerical study. *Langmuir* **2007**, *23*, 5896–5905.
46. Kibbe, W.A. OligoCalc: An online oligonucleotide properties calculator. *Nucleic Acids Res.* **2007**, *35*, W43–W46.